

**LEVEL II**

(12)  
13

Lee 1473

AD A090155

**Project Report**

TST-43

R. D'Amato

**Error Analysis of Pursuit  
and Proportional Navigation  
Control Laws**

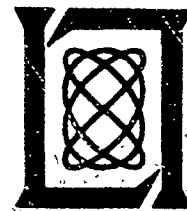
28 January 1980

Prepared for the Department of the Air Force  
under Electronic Systems Division Contract F19628-80-C-0002 by

**Lincoln Laboratory**

MASSACHUSETTS INSTITUTE OF TECHNOLOGY

LEXINGTON, MASSACHUSETTS



Approved for public release; distribution unlimited.

DTIC  
ELECTE  
S OCT 14 1980 D

A

80 10 10 087

DDC FILE COPY

MASSACHUSETTS INSTITUTE OF TECHNOLOGY  
LINCOLN LABORATORY

ERROR ANALYSIS OF PURSUIT  
AND PROPORTIONAL NAVIGATION CONTROL LAWS

*R. D'AMATO, Consultant*

*Group 44*

PROJECT REPORT TST-43  
(Tactical Systems Technology)

28 JANUARY 1980

Approved for public release; distribution unlimited.

LEXINGTON

MASSACHUSETTS



## 1.0 INTRODUCTION

This report describes a study which had as its objective the evaluation of pursuit and proportional navigation laws for use in closed loop simulations to develop/evaluate new techniques for emitter homing [1]. The use of a pursuit guidance law was a potential candidate since only stationary targets are considered. For targets which have a significant velocity proportional navigation has long been considered the acceptable approach [2, 3]. There have been other guidance laws which have been considered including modern optimum control schemes [2, 3]. However, these two laws with their variations, adaptations and extensions cover a broad class of useage. In addition, their simplicity (as compared with many "optimal" systems) allow a good understanding of their structure and operation. Furthermore, many of the modern control laws can be considered as "augmented" proportional navigation. Finally, proper use of these laws result in systems which can admit fairly wide variations in parameters without serious degradation of performance from the nominal design conditions.

One of the important aspects of this study is that the sensor used as the control element is likely to be a strapdown type, that is it is fixed to the body of the vehicle. It is important to note the ramifications that this has on the mechanization of the control system and, hence, its sensitivity to the motions of the vehicle, which can be quite large. This is in contrast to many situations in which the homing sensor is gimbal mounted, isolating it from body motion.

For this study, a framework has been selected which is relatively simple yet includes the essential features of the two control laws. Provision has been made to introduce the major physical parameters of a homing flight vehicle including its inertial and aerodynamic properties as well as a representation of the stability augmentation features of the autopilot, i.e., rate gyro and accelerometer feedback. For the present, the response has been limited to the linear regime for the final 10 seconds of flight, in which the velocity and aerodynamic parameters can be reasonably considered constant (except for the closing range between the vehicle and target).

The two types of error models used are described in Section 2.0. The first is a deterministic model in which a systematic external disturbance or an internal instrumentation error is introduced and the resulting response of the system is computed. The second is a stochastic model in which the external disturbances are characterized by their spectrum levels. The stochastic model utilizes an adjoint technique [5] in which the sensitivity of the system to various types of errors are computed.

In Section 3.0 numerical results of six types of vehicles are presented. (Note that the use of type includes the pitch and yaw characteristics of the vehicle, if they are different.) The tables of error coefficients allow various combinations of error levels to be studied and an overall miss-distance in feet to be computed.

Finally, in Section 4.0 some conclusions based on the numerical results are presented.

## 2.0 ERROR MODELS

### 2.1 Deterministic

The coordinate system with the vehicle is shown in Fig. 2.1. For our analysis small angles are assumed, that is

$$\cos \gamma \approx 1$$

$$\cos \theta \approx 1$$

$$\cos \alpha \approx 1$$

$$\lambda = \frac{-z}{V(t_0 - t)}$$

where  $\gamma$  = flight path angle

$\theta$  = body angle

$\alpha$  = angle of attack

$\lambda$  = line-of-sight (LOS) angle

Since we will be considering only the last 10 seconds of flight it is also reasonable to assume that the velocity is constant.

The equations of motion of the vehicle are

$$-m\dot{v} = L$$

$$J\dot{Q} = M$$

where  $L$  = aerodynamic lift

$m$  = mass (=  $W/g$ ) (slugs)

$W$  = weight (lbs)

$g$  = acceleration of gravity (=  $32.2 \text{ ft/sec}^2$ )

$J$  = moment of inertia

$$Q = \dot{\theta}$$

$M$  = aerodynamic moment

The lift and moment can be expressed as

$$\frac{L}{m} = Z_{\alpha} \alpha + Z_{\delta} \delta$$

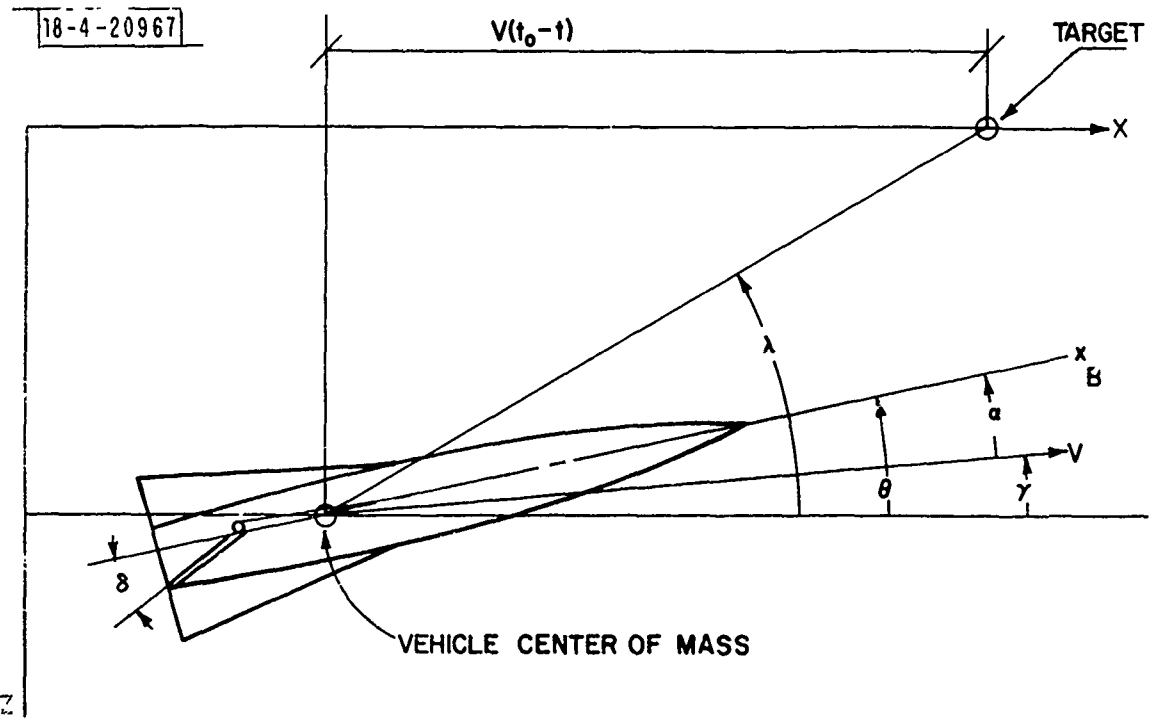


Fig. 2.1. Coordinate system.

$$\frac{M}{J} = M_{\alpha}\alpha + M_{\delta}\delta + M_Q Q$$

where

$$Z_{\alpha} = C_{L\alpha} q \text{ S/m}$$

$$Z_{\delta} = C_{L\delta} q \text{ S/m}$$

$$M_{\alpha} = C_{m\alpha} q \text{ S}\ell/J$$

$$M_{\delta} = C_{m\delta} q \text{ S}\ell/J$$

$$M_Q = C_{mQ} q \text{ s}(\ell^2/2V)/J$$

$\alpha$  = angle of attack

$$q = 1/2\rho v^2$$

$\delta$  = control surface rotation

$\rho$  = air density slugs/ft<sup>3</sup> (= 0.00238 at sea level)

S = reference area (ft<sup>2</sup>)

$\ell$  = reference length (ft)

$C_{L\alpha}$  = lift curve slope (per radian)

$C_{L\delta}$  = lift from control surface deflection (per deg)

$C_{m\alpha}$  = change of moment with angle of attack

$C_{m\delta}$  = change of moment with control surface deflector

$C_{mQ}$  = change of moment due to body rotation

For the small angle assumption

$$\ddot{Z} = -V \dot{\gamma} = -V(\dot{\theta} - \dot{\alpha})$$

Using the definition of angle-of-attack as

$$\alpha = \frac{u}{V}$$

where u is the lateral motion of vehicle in body coordinates. Thus

$$\ddot{Z} = \dot{u} - VQ$$

The equations of motion then become

$$\begin{aligned}\ddot{z} &= \dot{u} - VQ = Z_{\alpha}\alpha + Z_{\delta}\delta \\ \dot{Q} &= M_{\alpha}\alpha + M_{\delta}\delta + M_Q Q\end{aligned}$$

The control of the vehicle is accomplished through the control surface as

$$\delta = \delta_N + K_Q Q + kK_A \ddot{z}$$

where  $\delta_N$  is the control surface commanded by the navigation signal and the remaining two terms represent the autopilot function:  $K_Q$  is the rate damping and  $kK_A$  is acceleration feedback.

For pursuit navigation we have

$$\delta_N = -G_2 K_a [\hat{\lambda} - \theta]$$

where the hat ( ^ ) over the LOS angle in the brackets indicates a filtered estimate of the angular deviation from the desired direction of flight.

For proportional navigation

$$\delta_N = -G_1 K_A \hat{\lambda}$$

where the control signal is the filtered LOS rate.

The block diagram for the pursuit case is shown in Fig. 2.2 and for the proportional case in Fig. 2.3. As may be seen there are four error inputs:

1. Wind disturbance,  $\epsilon_W$ . The wind disturbance can take the form of any distribution. For example, for a wide band gaussian fluctuation the filter (bandwidth,  $\omega_W$ ) will produce a reasonable representation of the wind gust if the bandwidth is properly selected. With a wide bandwidth a fairly pure wind shear disturbance can be introduced into the system. For the models shown in Figs. 2.2 and 2.3, a wind shear of 1 ft/sec/100 ft will be used to generate the basic sensitivity of the system to winds. In terms of the time history, the wind shear can be expressed as  $E_W = 0.01 Vt$ .
2. Gyro error,  $\epsilon_G$ . For the pursuit navigation case the gyro error enters only through the feedback path of the autopilot. On the other hand, for proportional navigation case it enters not only into the damping feedback, but also into the command loop. The rate gyro signal is integrated to obtain a measure of the body attitude,  $\theta_M$ , which is subtracted from the LOS measurement from





the sensor giving:

$$\text{LOS} = (\theta - \lambda) - \theta_M$$

or

$$\text{LOS} = -\lambda + \epsilon_G$$

where  $\epsilon_G$  is the difference between the actual body position and that estimated from the rate gyro signal. Thus, in the block diagram,  $X_7$  represents the error  $\theta_G$ . For the basic sensitivity analysis the error will be computed on the basis of a gyro error of  $1^\circ/\text{sec}$ .

3. Sensor error,  $\epsilon_S$ . The sensor error can be a noise, drift or bias. The noise portion of the error will be considered below where the stochastic model is described. The deterministic error is assumed to be a bias of  $1^\circ$  for establishing the basic error sensitivity for deterministic errors.
4. Accelerometer error,  $\epsilon_A$ . The accelerometer error enters the feedback path of the acceleration autopilot loop. For some of the cases there will be no accelerometer, therefore,  $k = 0$  and there will be no acceleration error. The noise component will be considered below and the steady state level will be a bias of  $1 \text{ ft}/\text{sec}^2$  (about 30 millig's).

The sensor transfer function is assumed to be

$$H_S(S) = \frac{1}{\left(\frac{S}{\omega_S} + 1\right)^2}$$

for the pursuit case and

$$H_S(S) = \frac{S}{\left(\frac{S}{\omega_S} + 1\right)^2}$$

for the proportional case, where  $S$  is the Laplacian operator.

The equations represented by the block diagram can be cast into a matrix equation as

$$\dot{X} = FX + Gc$$

where the definitions of the components of this matrix equation are given in Tables 2.1 and 2.2 for pursuit and proportional cases, respectively.

TABLE 2.1

SUMMARY OF PURSUIT NAVIGATION EQUATIONS

$$\dot{x} = Fx + G\epsilon$$

<u>x<sub>8x1</sub></u>	<u>ε<sub>4x1</sub></u>	<u>G<sub>8x4</sub></u>
x <sub>1</sub> = z	ε <sub>1</sub> = ε <sub>W</sub>	G <sub>23</sub> = k K <sub>A</sub> Z <sub>δ</sub> Δ
x <sub>2</sub> = $\dot{z}$	ε <sub>2</sub> = ε <sub>S</sub>	G <sub>24</sub> = K <sub>Q</sub> Z <sub>δ</sub> Δ
x <sub>3</sub> = u	ε <sub>3</sub> = ε <sub>A</sub>	G <sub>33</sub> = k K <sub>A</sub> Z <sub>δ</sub> Δ
x <sub>4</sub> = Q	ε <sub>4</sub> = ε <sub>G</sub>	G <sub>34</sub> = K <sub>Q</sub> Z <sub>δ</sub> Δ
x <sub>5</sub> = λ <sub>1</sub>		G <sub>43</sub> = k K <sub>A</sub> M <sub>δ</sub>
x <sub>6</sub> = λ <sub>2</sub>		G <sub>44</sub> = K <sub>Q</sub> M <sub>δ</sub>
x <sub>7</sub> = θ		G <sub>52</sub> = ω <sub>S</sub>
x <sub>8</sub> = U <sub>W</sub>		G <sub>81</sub> = ω <sub>W</sub>

F<sub>δxδ</sub>

$$F_{12} = 1$$

$$F_{23} = \frac{Z_\alpha}{V} \Delta, \quad F_{24} = K_Q Z_\delta \Delta, \quad F_{25} = G_2 K_A Z_\delta \Delta, \quad F_{28} = -F_{23}$$

$$F_{33} = \frac{Z_\alpha}{V} \Delta, \quad F_{34} = K_Q Z_\delta \Delta + V, \quad F_{35} = G_2 K_A Z_\delta \Delta, \quad F_{38} = -F_{33}$$

$$F_{43} = \frac{M_\alpha}{V} + \frac{Z_\alpha k K_A M_\delta}{V}, \quad F_{44} = M_Q + K_Q M_\delta \Delta, \quad F_{45} = G_2 K_A M_\delta \Delta, \quad F_{48} = -F_{43}$$

$$F_{55} = -\omega_S, \quad F_{56} = \omega_S$$

$$F_{61} = \frac{-\omega_S}{V t_1}, \quad F_{66} = -\omega_S, \quad F_{67} = \omega_S$$

$$F_{74} = 1$$

$$F_{88} = -\omega_W$$

$$\Delta = 1 + Z_\delta k K_A, \quad t_1 = t_0 - t \quad t_0 = \text{flight time}$$

TABLE 2.2

SUMMARY OF PROPORTIONAL NAVIGATION EQUATIONS

$$\dot{\mathbf{x}} = \mathbf{F}\mathbf{x} + \mathbf{G}\epsilon$$

<u><math>x_{8 \times 1}</math></u>	<u><math>\epsilon_{4 \times 1}</math></u>	<u><math>G_{8 \times 4}</math></u>	
$x_1 = z$	$\epsilon_1 = \epsilon_W$	$G_{23} = k K_A Z_\delta \Delta$	
$x_2 = \dot{z}$	$\epsilon_2 = \epsilon_S$	$G_{24} = K_Q Z_\delta \Delta$	
$x_3 = U$	$\epsilon_3 = \epsilon_A$	$G_{33} = k K_A Z_\delta \Delta$	
$x_4 = Q$	$\epsilon_4 = \epsilon_G$	$G_{34} = K_Q Z_\delta \Delta$	
$x_5 = \lambda_1$		$G_{43} = k K_A M_\delta$	
$x_6 = \lambda_2$		$G_{44} = K_Q M_\delta$	
$x_7 = \epsilon_G$		$G_{52} = \omega_S^2$	$G_{62} = -\omega_S$
$x_8 = U_W$		$G_{74} = 1$	
		$G_{81} = \omega_W$	

 $F_{8 \times 8}$ 

$$F_{12} = 1$$

$$F_{23} = \frac{Z_\alpha \Delta}{V}, \quad F_{24} = K_Q Z_\delta \Delta, \quad F_{25} = G_1 K_A Z_\delta \Delta, \quad F_{27} = -F_{23}$$

$$F_{33} = F_{23}, \quad F_{34} = F_{24} + V, \quad F_{35} = G_1 K_A Z_\delta \Delta, \quad F_{37} = -F_{33}$$

$$F_{43} = \frac{M_\alpha}{V} + \frac{Z_\alpha}{V} k K_A M_\delta, \quad F_{44} = K_Q M_\delta \Delta + M_Q, \quad F_{45} = G_1 K_A M_\delta \Delta$$

$$F_{47} = -F_{43}$$

$$F_{51} = \frac{-\omega_S^2}{V(t_0 - t)}, \quad F_{55} = -\omega_S, \quad F_{56} = \omega_S^2, \quad F_{57} = -\omega_S^2$$

$$F_{61} = \frac{\omega_S}{V(t_0 - t)}, \quad F_{66} = -\omega_S, \quad F_{67} = \omega_S, \quad F_{88} = -\omega_W$$

$$t_0 = \text{flight time} \quad \Delta = 1 + k K_A Z_\delta$$

The numerical solution of these equations can be expressed as

$$x_n = (I + \Delta t F_n) X_{n-1} + \Delta t G \epsilon_n$$

where I is an identify matrix and  $\Delta t$  is the solution time interval.

## 2.2 Stochastic

The sensitivity of the miss distance to stochastic inputs is most conveniently done using the adjoint technique [5]. Basically, this technique recasts the block diagram of the basic system into an adjoint form by

1. replacing  $t$  by  $t_0 - t$  in the arguments of all time varying coefficients where  $t_0$  is the final flight time
2. reversing all signal flow, redefining branch points as sum points and sum points as branch points, making the original inputs appear as outputs in the adjoint system.

Before going on to the more complex problem we will consider a simple system to illustrate the adjoint technique. Figure 2.4 shows a second order system with its adjoint. The system is excited by a white noise input  $\epsilon$  having a spectral density of  $\Phi$  units<sup>2</sup>/Hz. The rms response to the basic system is given as:

$$\sigma_{x_1}^2 = \frac{1}{2\pi} \int_{-\infty}^{\infty} |H(\omega)|^2 d\omega$$

where  $H(\omega) = \frac{\omega_0^2}{\omega_0^2 - \omega^2 + 2\zeta\omega_0 j\omega}$ . Carrying out the integration we obtain the

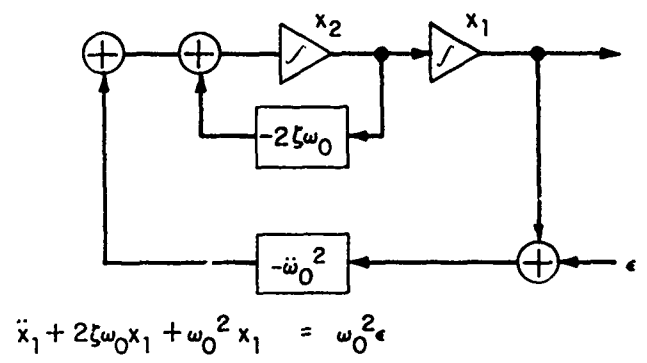
classic result

$$\sigma_{x_1}^2 = \frac{\omega_0^2}{4\zeta}$$

For the adjoint problem the solution is expressed as

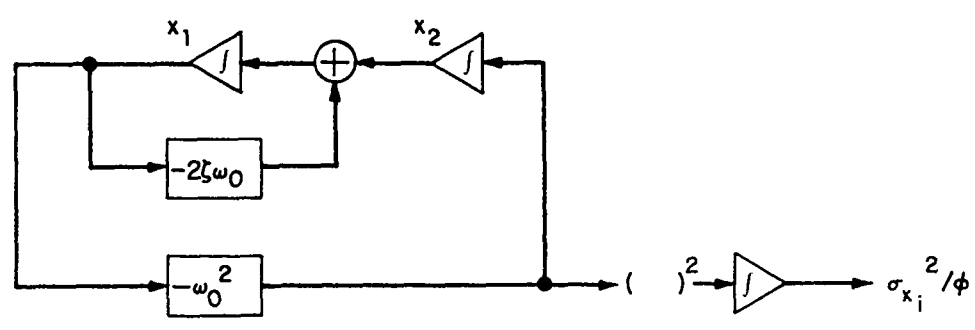
$$\sigma_{x_1}^2 = \Phi \int_0^t \omega_0^4 x_1^2 dt$$

18-4-20970



$$\ddot{x}_1 + 2\zeta\omega_0\dot{x}_1 + \omega_0^2 x_1 = \omega_0^2 \epsilon$$

(a)



$$\ddot{x}_1 + 2\zeta\omega_0\dot{x}_1 + \omega_0^2 x_1 = 0$$

$$\sigma_{x_1}^2 / \Phi = \int_0^{\infty} \omega_0^4 x_1^2 dt$$

(b)

Fig. 2.4(a&b). Illustration of basic system with its adjoint excited by white noise signal ε with spectral density φ.

where  $x_1 = \frac{1}{\beta} e^{-\zeta\omega_0 t} \sin\beta t$ ,  $\beta = \omega_0 \sqrt{1-\zeta^2}$  for initial condition of  $\dot{x}_1(0) = 1$ ,  $x_1(0) = 0$  (or the impulse response).

Carrying out the integration we get

$$\sigma_{x_1}^2 = \Phi \left\{ \frac{\zeta\omega_0}{2(1-\zeta^2)} \sin^2 \beta t - \frac{\omega_0}{2\sqrt{1-\zeta^2}} \sin\beta t \cos\beta t \right\} e^{-2\zeta\omega_0 t} - \Phi \left\{ \frac{\omega_0}{4\zeta} (e^{-2\zeta\omega_0 t} - 1) \right\}$$

which is the adjoint time history of the variance of  $x_1$ . It is readily seen that as  $2\zeta\omega_0 t$  becomes large, we obtain the steady state result.

$$\sigma_{x_1}^2 = \frac{\omega_0}{4\zeta} \Phi$$

The usefulness of the adjoint technique becomes apparent for more complex systems with multiple stochastic inputs. Not only are all the sensitivities to the inputs determined in one run, but the stability of the system may also be observed.

Although the adjoint technique can handle nonlinearities [5], only linear cases will be considered in the present study.

Using the two rules for obtaining an adjoint block diagram for a specific system, the pursuit and proportional navigation were obtained as shown in Figs. 2.5 and 2.6. From these block diagrams, the equations for both systems were obtained in the form

$$\begin{aligned} \dot{x} &= F^A x \\ \dot{s} &= S_D^2 \end{aligned}$$

where the  $x$  is a  $9 \times 1$  vector. The  $F^A$  is the system adjoint matrix with dimensions appropriate to the  $x$  vector. The second equation is a vector equation for the outputs in terms of the solution vector,  $x$ . It is of  $4 \times 1$  dimension to account for the four output variances (stochastic inputs for the original sys-

TABLE 2.3

SUMMARY OF PURSUIT NAVIGATION EQUATIONSADJOINT SYSTEM

$$\dot{\mathbf{x}} = \mathbf{F}^A \mathbf{x} \quad \dot{\mathbf{s}} = \mathbf{S}_0^2$$

$$\begin{aligned} S_1 &= \sigma_w^2 / \phi_w & S_{01} &= \omega_w x_8 \\ S_2 &= \sigma_s^2 / \phi_s & S_{02} &= \omega_w x_6 \\ S_3 &= \sigma_A^2 / \phi_A & S_{03} &= z_\delta k K_A \Delta (x_2 + x_3) + k K_A M_\delta x_4 \\ S_4 &= \sigma_G^2 / \phi_G & S_{04} &= x_9 / t_G \end{aligned}$$

$$F_{16}^A = \frac{-\omega_s}{Vt}$$

$$F_{21}^A = 1$$

$$F_{32}^A = \frac{z_\alpha}{V} \Delta, \quad F_{33}^A = \frac{z_\alpha}{V} \Delta, \quad F_{34}^A = \frac{M_\alpha}{V} + \frac{M_\delta k K_A z_\delta}{V}$$

$$F_{42}^A = z_\delta K_Q \Delta, \quad F_{43} = F_{42} + V, \quad F_{44}^A = M_Q + M_\delta K_Q \Delta, \quad F_{47}^A = 1$$

$$F_{52}^A = z_\delta K_A G_2 \Delta, \quad F_{53}^A = F_{52}^A, \quad F_{54}^A = M_\delta K_A G_2 \Delta, \quad F_{55}^A = -\omega_s$$

$$F_{65}^A = \omega_s, \quad F_{66}^A = -\omega_s$$

$$F_{76}^A = \omega_s$$

$$F_{82}^A = -F_{32}^A, \quad F_{83}^A = F_{82}^A, \quad F_{84}^A = -F_{34}^A, \quad F_{88}^A = -\omega_w$$

$$F_{99}^A = -\frac{1}{t_G}, \quad F_{92}^A = K_Q Z_\delta \Delta, \quad F_{93}^A = F_{92}^A, \quad F_{94}^A = K_Q M_\delta \Delta$$

$$\Delta = 1 + k K_A z_\delta$$

TABLE 2.4

SUMMARY OF PROPORTIONAL NAVIGATION EQUATIONSADJOINT SYSTEM

$$\dot{x} = F^A x \quad \dot{s} = S_0^2$$

$$S_1 = \sigma_w^2 / \phi_w$$

$$S_{01} = \omega_w x_7$$

$$S_2 = \sigma_S^2 / \phi_S$$

$$S_{02} = \omega_S^2 x_5 - \omega_S x_6$$

$$S_3 = \sigma_A^2 / \phi_A$$

$$S_{03} = z_\delta k K_A \Delta (x_2 + x_3) + k K_A M_\delta x_4$$

$$S_4 = \sigma_G^2 / \phi_G$$

$$S_{04} = x_9 / \tau_G$$

$$F_{15}^A = \frac{-\omega_S^2}{Vt}$$

$$F_{16}^A = \frac{\omega_S}{Vt}$$

$$F_{21}^A = 1$$

$$F_{32}^A = \frac{z_\alpha}{V} \Delta, \quad F_{33}^A = F_{32}^A, \quad F_{34}^A = \frac{M_\alpha}{V} + \frac{M_\delta k K_A z_\delta}{V}$$

$$F_{42}^A = z_\delta K_Q \Delta, \quad F_{43}^A = V + F_{42}^A, \quad F_{44}^A = M_\delta K_Q \Delta + M_Q$$

$$F_{52}^A = z_\delta K_A G_1 \Delta, \quad F_{53}^A = F_{52}^A, \quad F_{54}^A = M_\delta K_A G_1 \Delta, \quad F_{55}^A = -\omega_S$$

$$F_{65}^A = \omega_S^2, \quad F_{66}^A = -\omega_S, \quad F_{75}^A = -\omega_S^2, \quad F_{76}^A = \omega_S$$

$$F_{82}^A = -F_{32}^A, \quad F_{83}^A = F_{82}^A, \quad F_{84}^A = -F_{34}^A, \quad F_{88}^A = -\omega_w$$

$$F_{99}^A = -1/\tau_g, \quad F_{92}^A = K_Q z_\delta \Delta, \quad F_{97}^A = 1, \quad F_{93}^A = F_{92}^A, \quad F_{94}^A = K_Q M_\delta \Delta$$

$$\Delta = 1 + k K_A z_\delta$$

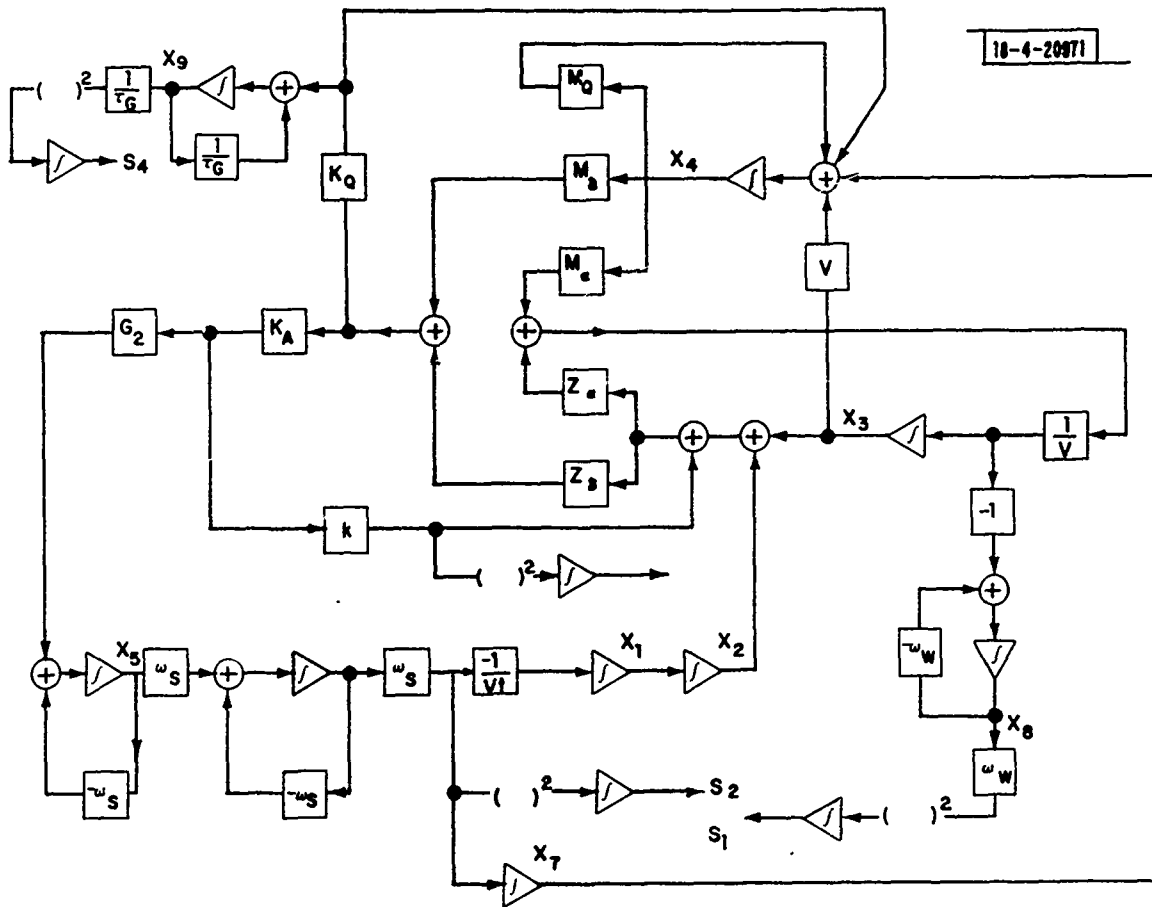


Fig. 2.5. Adjoint pursuit navigation model.

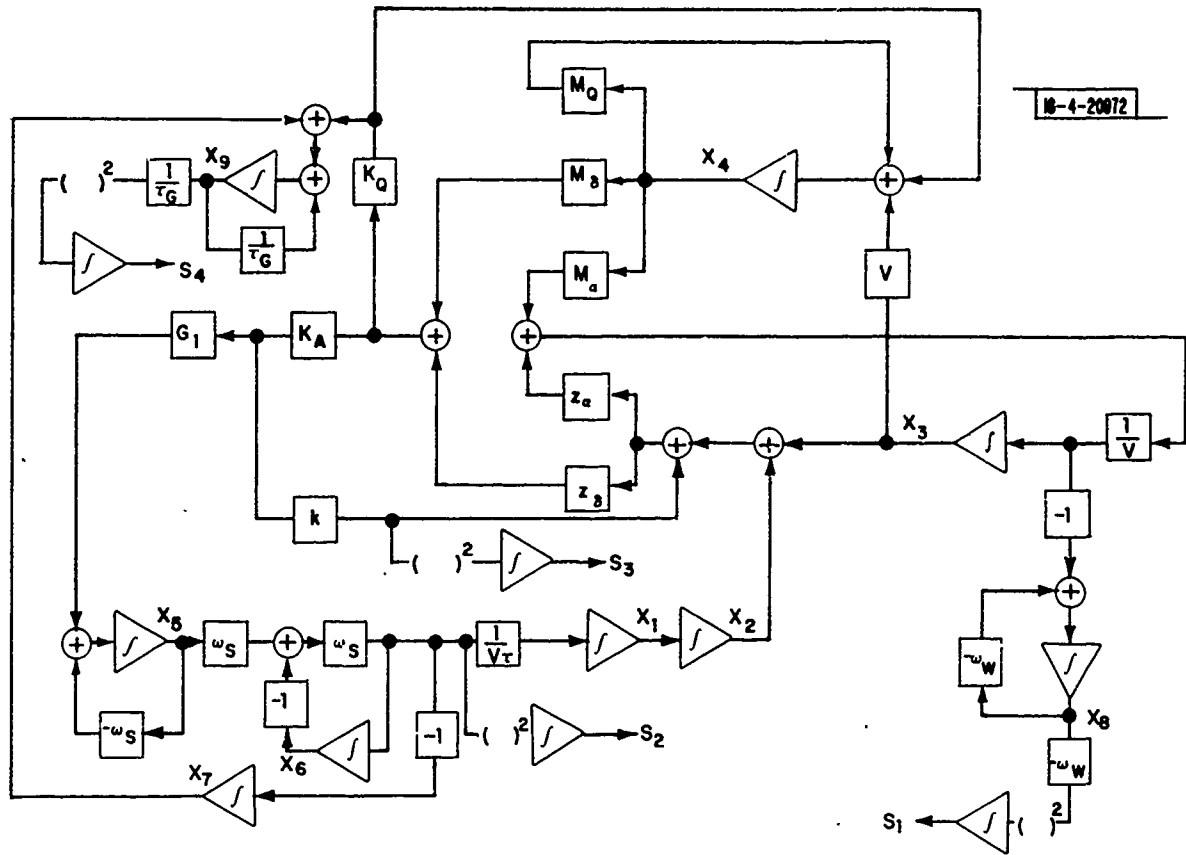


Fig. 2.6. Adjoint proportional navigation model.

tem). The details of the equations are given in Tables 2.3 and 2.4 for pursuit and proportional, respectively. It is noted that a filter has been added between the gyro noise output and the system. This is to account for the reasonable long correlation times that can exist for gyro noise.

Solution of these equations is carried out by seeking the impulsive condition on miss distance which can be accomplished by giving an initial condition of  $\dot{z}(0) = 1$  and propagating the results for the solution time, which was taken as 10 seconds for all cases run. As for the basic system described above, these equations were solved numerically as

$$x_n = (I - \Delta t F_A) x_{n-1}$$

$$S_n = S_{n-1} + \frac{\Delta t}{2} (S_{o_n}^2 + S_{o_{n-1}}^2)$$

with  $\Delta t = 0.01$  second and initial condition  $x_2(0) = 1$ . To obtain variance of the miss distance from all four error sources we multiply each output by its spectral density as

$$\sigma^2 = S_1 \phi_w + S_2 \phi_S + S_3 \phi_A + S_4 \phi_G$$

where the subscripts are wind, sensor, accelerometer, and gyro, respectively. In the case of the wind spectrum we have

$$\phi_w = \frac{2\sigma_w^2}{\omega_w}$$

where  $\sigma_w$  is the rms level of wind gust

$$\omega_w = V/L_w$$

$L_w$  is the wind correlation length

$V$  is the vehicle velocity.

Thus, an error budget for the system is quite readily obtained.

### 3.0 NUMERICAL RESULTS

Calculations for both pursuit and proportional navigation laws were carried out for six representative flight models.

MISSILE - is a boost-glide vehicle with a speed less than Mach 1 in the terminal phase of the flight. Since it is symmetrical, both pitch and yaw are essentially the same. The characteristics are similar to the Maverick missile.

PROJECTILE - is based on a 155 mm cannon launched projectile which deploys a set of fins and wings for control. It also has a speed less than Mach 1 in the terminal phase of flight. As for the missile, it also is symmetrical.

MINI DRONE - is a representative version of a powered mini drone. The vehicle considered in this study is a skid-to-turn vehicle with side force surfaces for enhanced yaw steering capacity. Its pitch and yaw dynamic characteristics are substantially different from one another so both pitch and yaw models are considered.

GLIDE BOMB - bears a representative likeness to the GBU-15 planar wing glide bomb. It also is a skid-to-turn vehicle but with no enhancing side force surfaces. The pitch and yaw characteristics are sufficiently different from one another so that each is considered as a separate case in the error studies.

Table 3.1 gives the numerical parameters [6] for the six cases studied. The yaw parameters have been modified in sign to allow the equations developed in Section 2.0 to be used. The flight characteristics of each vehicle required stability augmentation to be adequate for the application. Representative values of feedback gains were selected to represent this stability augmentation or autopilot function:

$K_Q$  is a rate gyro which senses the body rate and supplies a signal to the control surface to oppose body motion and, thus, provides additional damping.

$k$  is an accelerometer which senses the body acceleration and provides a signal to the control surface which is used to null the difference between commanded acceleration and actual body acceleration. For the Projectile and Mini Drone, there is no accelerometer so that the gain is taken to be zero.

$K_A$  is the gain which converts the commanded acceleration into a control surface position

TABLE 3.1

PARAMETERS FOR ERROR ANALYSIS

	MISSILE	PROJECTILE	MINI DRONE		GLIDE BOMB	
			(PITCH)	(YAW)	(PITCH)	(YAW)
S (FT <sup>2</sup> )	0.786	0.196	18.18	18.18	16.6	16.6
W (LBS)	398	135	135	135	3000	3000
J (SLUG FT <sup>2</sup> )	53.5	6.13	25.5	32.4	646.2	716.6
V (FT/SEC)	700	800	200	200	600	600
ℓ (FT)	1	0.5	1.65	1.65	1.54	11.33
L <sub>w</sub> (FT)	900	900	900	900	900	900
C <sub>Lα</sub> (/RAD)	-14.32	-20.05	-5.5	-1.5	-5.73	-1.66
C <sub>Lδ</sub> (/DEG)	-0.066	-0.130	-0.0066	-0.0044	-0.008	-0.015
C <sub>Mα</sub> (/RAD)	-6.99	-19.19	-1.72	-0.80	-0	-0
C <sub>Mδ</sub> (/DEG)	-0.230	-0.390	-0.0223	-0.140	-0.038	-0.006
C <sub>MQ</sub> (/RAD)	-573	-155	-7.0	-10.0	-0	-0
k	-1	0	0	0	-1	-1
K <sub>A</sub> (D/FT/S <sup>2</sup> )	2.2/g	2/g	2/g	2/g	2/g	2/g
K <sub>Q1</sub> (D/R/S)	0.2*r	0.2*r	0.2*r	0.2*r	0.2*r	0.2*r
K <sub>Q2</sub> (D/R/S)	0.3*r	0.3*r	0.2*r	0.2*r	0.3*r	0.5*r
G <sub>1</sub> <sup>Q2</sup> (F/S <sup>2</sup> /R/S)	6V	6V	6V			
G <sub>2</sub> <sup>1</sup> (F/S <sup>2</sup> /R)	5V					
ω <sub>S1</sub> (R/S)	2π	2π	2π	2π	2π	2π
ω <sub>S2</sub> (R/S)	4π	4π	4π	4π	4π	4π
ω <sub>S2</sub> (RAD/S)	11.26	16.26	13.38	6.80	4.78	2.63
ζ <sub>1</sub> --	1.07	1.63	0.807	0.726	0.848	1.507
G <sub>1</sub> <sup>01</sup> (F/S <sup>2</sup> /R/S)	0.443	0.500	0.449	0.213	0.765	0.765
ω <sub>2</sub> (R/S)	11.55	16.73	13.38	6.80	5.05	3.06
ζ <sub>2</sub> --	1.49	2.36	0.807	0.726	1.167	3.188
G <sub>2</sub> <sup>02</sup> (FT/S <sup>2</sup> /R)	0.481	0.473	0.449	0.213	0.684	0.565

TABLE 3.2  
ERROR SENSITIVITIES

VEHICLE	PROPORTIONAL NAVIGATION				STOCHASTIC (3)				ZERO ERROR (4)
	DETERMINISTIC (2)		GYRO		WIND		ACCEL		
MISSILE	0.7	0.2	0.3	1.3	614	12.5 (5)	--	159	0.04
PROJECTILE	0.7	0.1	0.2	2.3	800	6.0	--	171	0.08
DRONE-PITCH	0.2	0.2	0.1	0.2	31	10.6	--	5.5	0.15
DRONE-YAW	--	0.5	--	0.8	46	7.6	--	14.8	0.15
GLIDE BOMB-PITCH	0.1	0.1	0.1	1.0	4000	139	0.4	1158	0.05
GLIDE BOMB-YAW	34	2.0	9.7	40.6	5700	1560	8.1	15484	0.33

VEHICLE	PURSUIT NAVIGATION				STOCHASTIC (3)				ZERO ERROR (4)
	DETERMINISTIC (2)		GYRO		WIND		ACCEL		
MISSILE	28.3	101	0.8	1.8	109	0.61	--	0.6	0.7
PROJECTILE	35.1	119	1.2	4.1	152	0.68	--	1.1	1.0
DRONE-PITCH	3.4	17	--	0.5	6	0.92	--	0.2	0
DRONE-YAW	8.0	31	0.3	1.7	10	0.33	--	0.3	0.3
GLIDE BOMB-PITCH	24.0	90	0.7	3.9	86	0.60	0.1	2.0	0.4
GLIDE BOMB-YAW	55.3	115	14.2	23.8	172	1.25	0.4	26.2	18.5

NOTES:

(1) INPUT VALUES FOR SENSITIVITY ANALYSIS

	DETERMINISTIC	STOCHASTIC
SENSOR	1 DEG	1 DEG <sup>2</sup> /HZ
WIND	1 FT/SEC/100 FT	1 FT/SEC (RMS)
ACCEL	1 FT/SEC <sup>2</sup>	1 (FT/SEC <sup>2</sup> ) <sup>2</sup> /HZ
GYRO	1 DEG/SEC	1 (DEG/SEC) <sup>2</sup> /HZ

- (2) MISS DISTANCE FT (10)
- (3) MISS DISTANCE FT<sup>2</sup>/SPECTRUM LEVEL
- (4) MISS DISTANCE FT
- (5) MISS DISTANCE FT<sup>2</sup>/SPECTRUM LEVEL
- (6) INITIAL CONDITION 10 FT/SEC FOR DETERMINISTIC CALCULATION

The dynamic characteristics of the vehicle autopilot were computed and are also included in Table 3.1. As may be seen, there is a wide variation in natural frequency from a high of about 16 radians/sec to a low of about 2.6 radians/sec, or a factor of 6. It is to be noted that there are differences between the dynamic characteristics of the vehicles in the pursuit mode from those in the yaw mode. The reason for this is that for an adequate behavior, the rate damping had to be greater for pursuit than for proportional, except for the mini drone. The aerodynamic gain varies from 0.276 to 0.77 at about a factor of three. The overall kinematic gain of the systems varies with time as

$$G_{\text{kinematic}} = \frac{G_{oi} \times \overline{G_i}}{t_o - t}$$

where  $i = 1$  is the proportional navigation case

$i = 2$  is the pursuit navigation case

$\overline{G_i} = G_i/V$  the navigation gain

$G_{oi}$  = aerodynamic gain

$t_o$  = flight time

Although the gains selected are not necessarily optimal, they do provide a reasonably good system response for no errors or disturbances.

The parameters of Table 3.1 were used in the numerical evaluation of the equations outlined in the previous section. As a baseline, the six vehicles were run for both proportional and pursuit with no errors or disturbances. Figures 3.1, 3.2, and 3.3 are typical responses of the cross range distance (miss distance) and lateral acceleration for the Missile, Mini Drone-pitch, and Glide Bomb-yaw, respectively. The initial condition in all cases was a 10 ft/sec cross range velocity,  $\dot{z}(o)$ , or an angular miss alignment of  $\dot{z}(o)/V$  for the vehicle. Except for the pursuit case of Glide Bomb-yaw, miss distances were small (as typified by the Missile and Mini Drone). Because of the poor Glide Bomb-yaw response characteristics, it is not too surprising that difficulties existed in this final 10 second flight period. It is further to be noted that the peak acceleration levels of the pursuit cases were constantly higher than for the proportional cases.

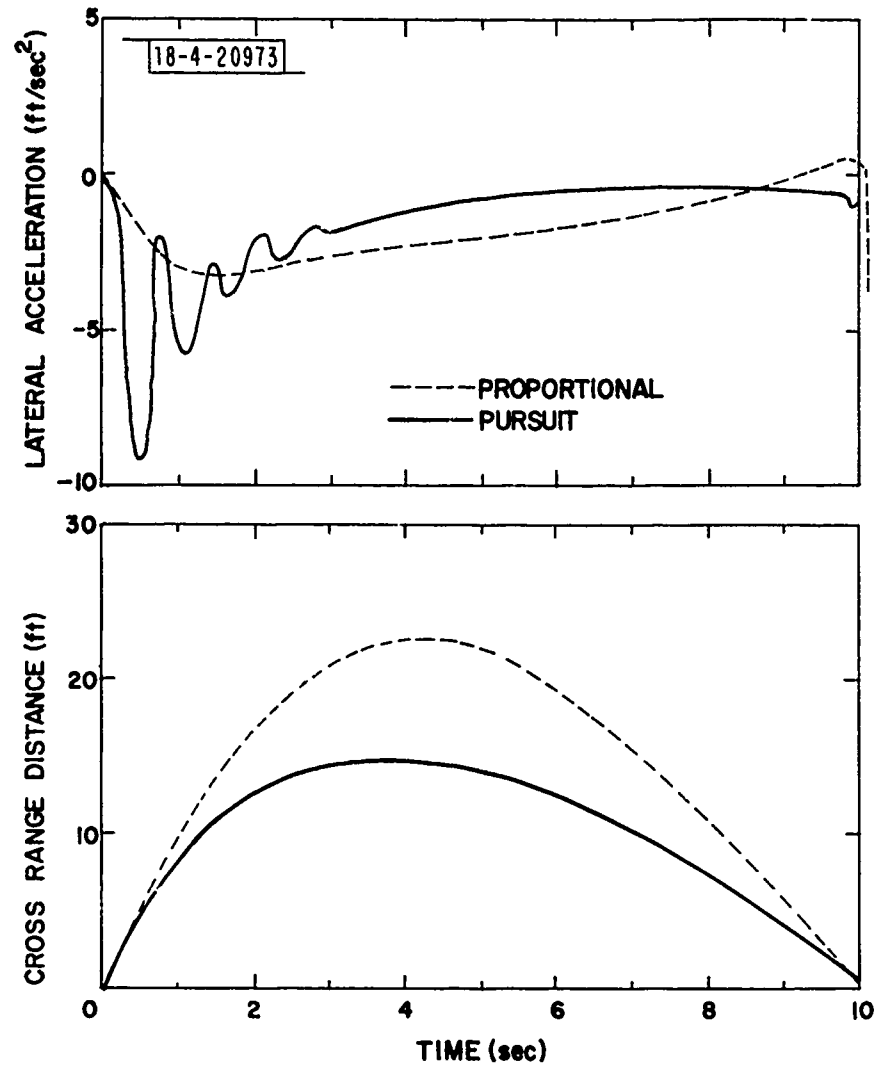


Fig. 3.1. Generic missile response for no errors - initial velocity = 10 ft/sec.

18-4-20974

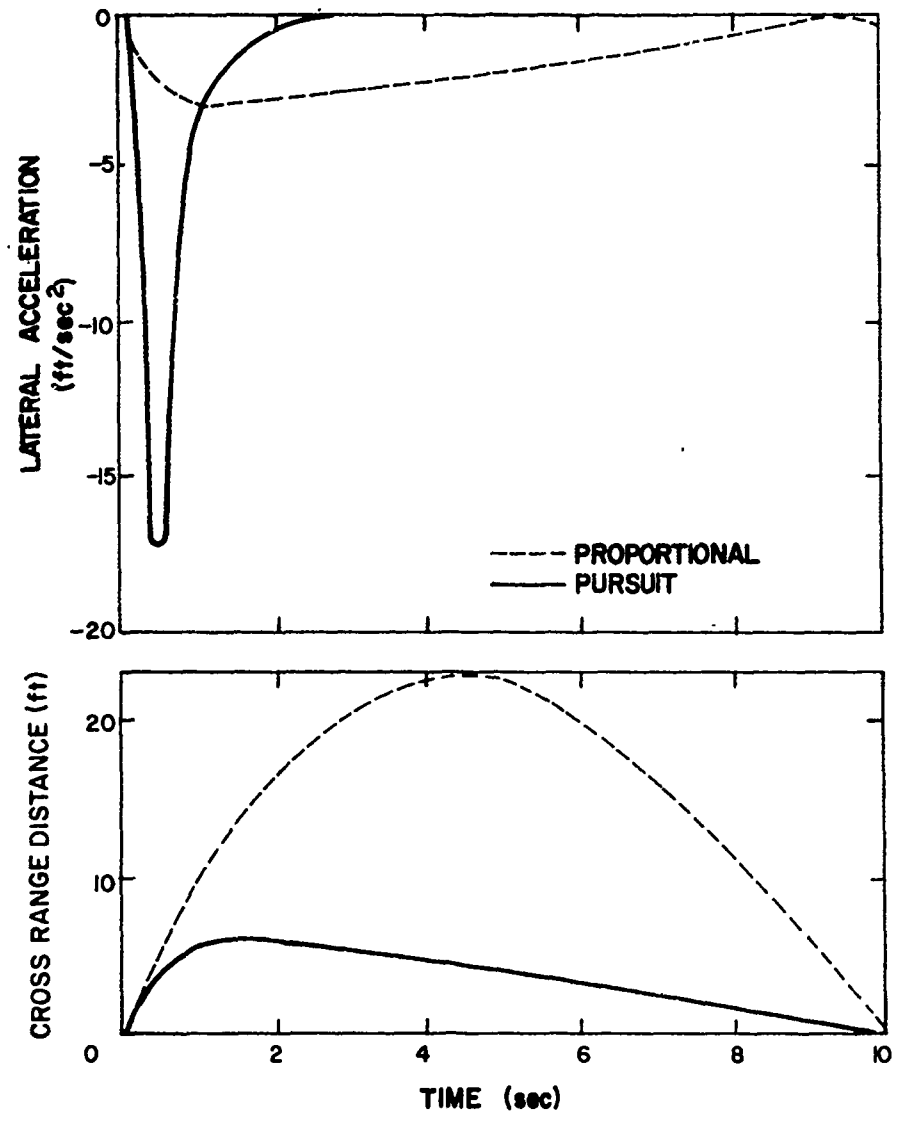


Fig. 3.2. Drone-Pitch response for no errors initial velocity 10 ft/sec.

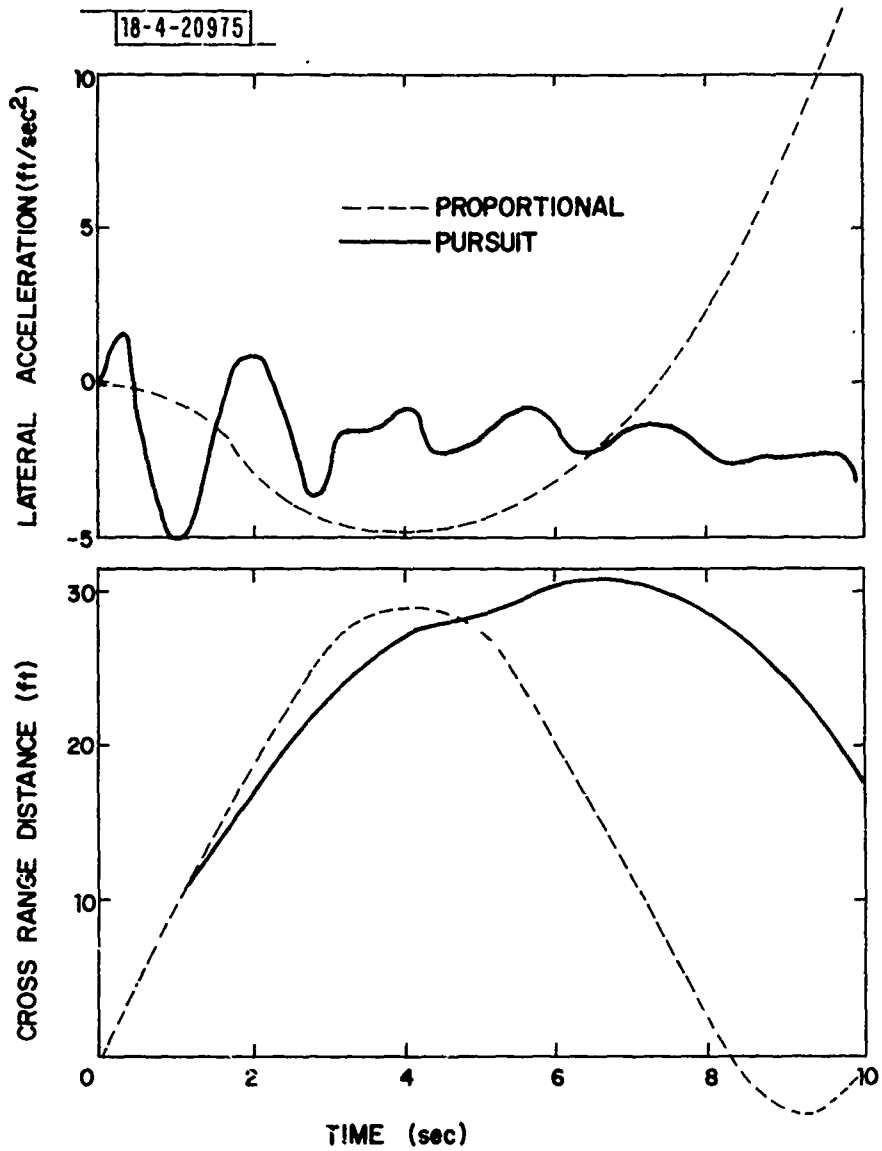


Fig. 3.3. Glide bomb-yaw response for no errors - initial velocity 10 ft/sec.

Table 3.2 gives a complete summary of the error sensitivities of the six vehicle types for both proportional and pursuit navigation. The two sections of the table are the basic error sensitivities for deterministic and stochastic inputs as discussed in the previous section. For the deterministic cases, the numbers represent the miss distance in feet due to a specific level of input as follows

SENSOR	- 1° (BIAS)
WINDSHEAR	- 1 ft/sec/100 ft.
ACCELEROMETER	- 1 ft/sec <sup>2</sup> (BIAS)
GYRO	- 1°/sec (BIAS)

For the stochastic cases, the values in the table represent the variance divided by the spectrum level as noted in the previous section.

In looking at the error sensitivities, certain patterns emerge for the two control laws. If we leave out the Glide Bomb-yaw case as being atypical, we notice that both accelerometer and gyro errors are relatively low contributors for both pursuit and proportional for deterministic inputs. On the other hand, the wind shear and sensor inputs are substantial contributors for pursuit and very small contributors for proportional. When we look at the stochastic inputs, we see that the major contributors for proportional are the sensor and the gyro. The reason for the large gyro contribution is due to the fact that the gyro is used to separate out the body position from the line-of-sight. The wind and accelerometer contributions are relatively small. For pursuit, the sensor is a moderate contributor while the wind gustiness is the major contributor.

Figure 3.4 illustrates some typical adjoint responses for the gyro noise error and proportional navigation. The data have been normalized with respect to the maximum values given in Table 3.2 (for example, 159 ft<sup>2</sup>/spectrum level for the missile). This figure provides a graphic illustration of the sluggishness of the Glide Bomb (particularly yaw) compared with the other vehicles.

It is further noted that the values for gyro noise given in Table 3.2 assume wide band input. These values are markedly reduced as the correlation

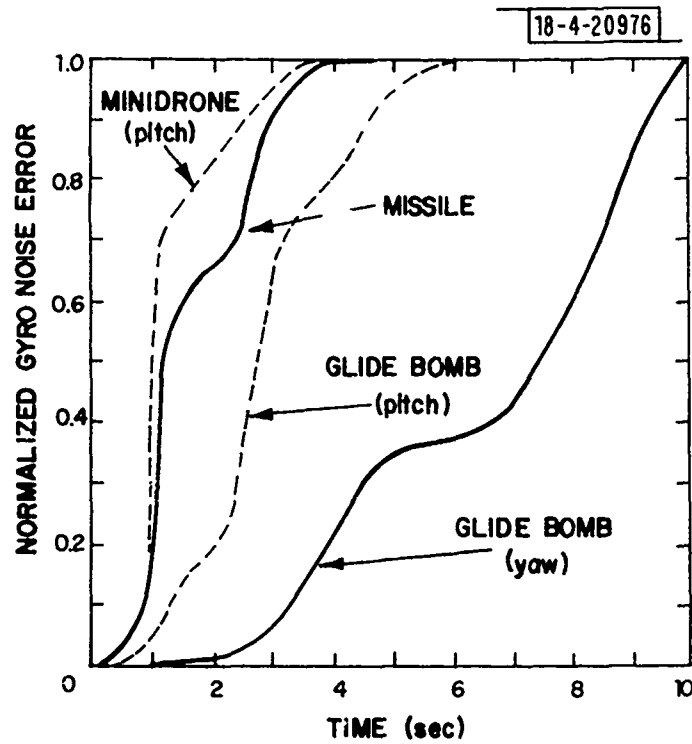


Fig. 3.4. Adjoint response of gyro noise error normalized to maximum value — proportional.

time increases. The relationship shown in Figure 3.5 can be expressed as

$$\left(\frac{\sigma_G^2}{\Phi_G}\right) = \frac{\left(\frac{\sigma_G^2}{\Phi_G}\right)_o}{1 + \tau_G^2}$$

where  $\left(\frac{\sigma_G^2}{\Phi_G}\right)_o$  is the value for the gyro noise in Table 3.2.

$\left(\frac{\sigma_G^2}{\Phi_G}\right)$  is the correlated value

$\tau_G$  is the correlation time of the gyro noise

This expression can be used for all of the vehicles as a reasonable approximation. The spectrum level for the gyro noise is given as

$$\Phi_G = 2 \sigma_G^2 \tau_G$$

To obtain a measure of overall performance, it is necessary to select some reasonable values of errors/disturbances. For the sensor, we have assumed a bias of 1 degree and noise level of  $0.08 \text{ deg}^2/\text{Hz}$ . For a bandwidth of 10 Hz this implies an rms value of about  $1.6^\circ$ . The wind shear was taken as  $0.5 \text{ ft/sec}/100 \text{ ft}$ . which implies a variation of 150 ft/sec from sea level to 30,000 ft. altitude (for the pitch plane). The gust intensity was chosen to be 10 ft/sec (rms), with the spectrum level being

$$\Phi_w = \frac{2 L_w (10)^2}{V} = \frac{200 L_w}{V}$$

where  $L_w$  is the correlation length assumed to be 900 ft. and V is the vehicle velocity. [7] suggests that an autopilot grade accelerometer will have a bias of 10 millig's (or  $0.32 \text{ ft/sec}^2$ ). For our analysis, we will assume a pessimistic value of  $1 \text{ ft/sec}^2$  bias. [8] suggests that autopilot grade accelerometers are an order of magnitude lower in accuracy than inertial grade, and that a noise spectrum level of 1 millig (or  $0.024 \text{ (ft/sec}^2)^2/\text{Hz}$ ) will be reasonably conservative.

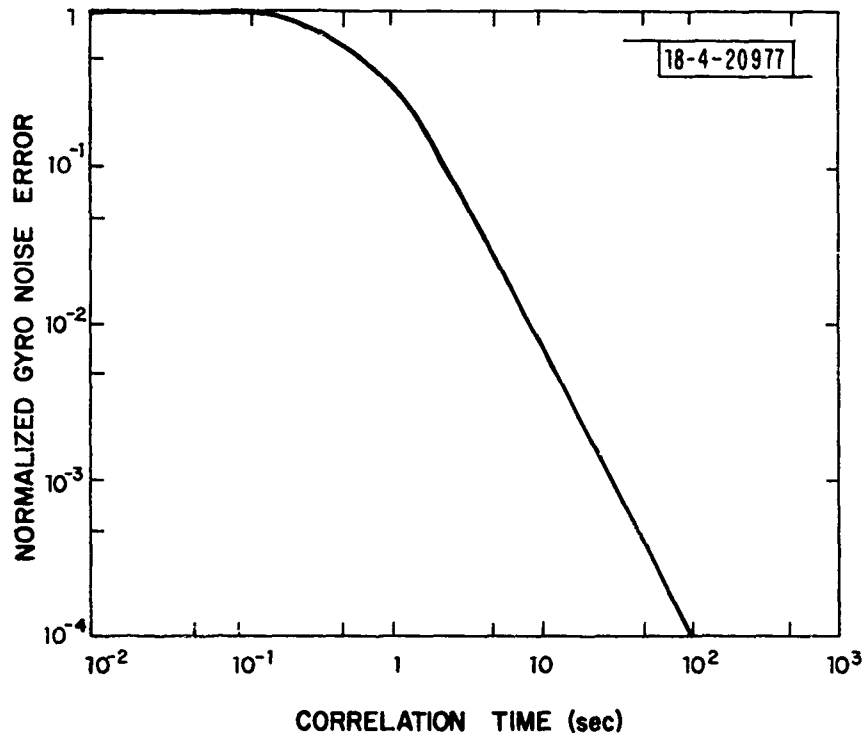


Fig. 3.5. Normalized gyro noise error as a function of correlation time.

[8] suggests that the drift or bias of an autopilot grade gyro will be two orders of magnitude worse than an inertial grade unit. Considering a 10-15 deg/h inertial grade gyro implies a bias level of about 0.35 deg/h for an autopilot grade gyro, which is in agreement with the range of autopilot grade gyros suggested by [7].

Finally, a chart in [7] suggests that for an inertial gyro an rms of 0.1°/h with a correlation time of 15 min. would be a reasonable noise level. Using a factor of 100 on each of these, we obtain a spectrum level of

$$G = 2 \left( \frac{10}{3600} \right)^2 (10) = 1.5 \times 10^{-4} \text{ (deg/sec)}^2/\text{Hz}$$

With a correlation time of 10 seconds, the reduction factor for the gyro noise sensitivity in Table 3.2 will be  $10^{-2}$ . These levels make the gyro noise contribution negligible.

The error budget using these values is summarized in the two sections of Table 3.3 for proportional and pursuit, respectively. The values for the individual components of the error budget are the 1 $\sigma$  miss distances in feet and the RSS error for each of the vehicles for each law is shown at the right hand side of the table. It can be seen that the RSS errors for proportional are consistently lower than for pursuit by a substantial measure. For proportional, the major contributor is the sensor, while for pursuit, the major contributors are the sensor bias, wind shear, and gust.

Although Table 3.3 does not seem to indicate so, gyro bias can be a substantial contributor to miss distance. The reason for this is demonstrated in Figure 3.6, which is a plot of cross range distance and lateral acceleration for the missile with a bias of 1°/sec in the gyro. The rather large excursions and acceleration introduced by this error stand out in comparison to the zero error case. The accelerations caused by gyro bias will produce a substantial increase in drag which will, in turn, reduce the speed of an unpowered vehicle. The reduced speed will reduce both range and maneuver capability, thereby increasing the potential to miss the target.

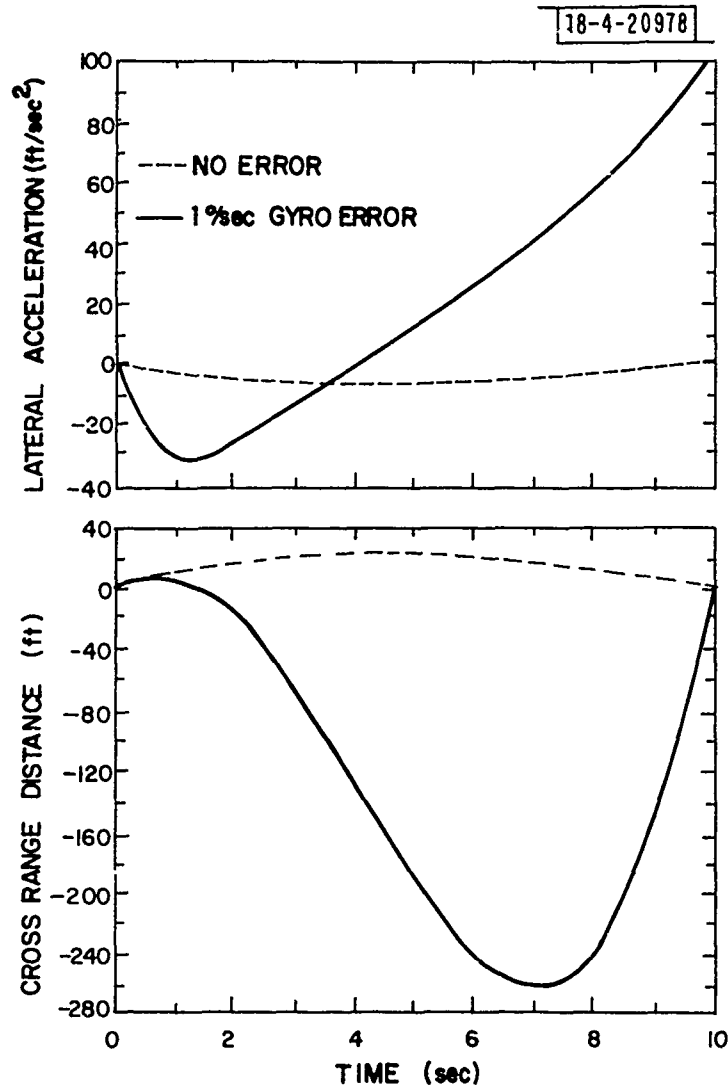


Fig. 3.6. Generic missile responses with and without bias error 10 ft/sec initial condition.

TABLE 3.3

ERROR SUMMARY

PROPORTIONAL NAVIGATION

VEHICLE	<u>DETERMINISTIC</u>					<u>STOCHASTIC</u>				
	SENSOR	WIND	ACCEL	GYRO	SENSOR	WIND	ACCEL	GYRO	RSS	
MISSILE	0.7 (1)	0.1	0.3	0.5	7.0	0.6	--	--	7	
PROJECTILE	0.7	--	0.2	0.8	8.0	0.4	--	--	8	
DRONE-PITCH	0.2	0.1	--	0.1	1.6	1.0	--	--	2	
DRONE-YAW	--	0.3	--	0.3	1.9	0.8	--	--	2	
GLIDE BOMB-PITCH	0.1	--	0.1	0.3	17.9	2.0	--	--	18	
GLIDE BOMB-YAW	34	1.0	10	15	21.3	6.8	0.4	--	48	

PURSUIT NAVIGATION

VEHICLE	<u>DETERMINISTIC</u>					<u>STOCHASTIC</u>				
	SENSOR	WIND	ACCEL	GYRO	SENSOR	WIND	ACCEL	GYRO	RSS	
MISSILE	28.3	50.7	0.8	0.8	2.9	12.5	--	0.1	59	
PROJECTILE	35.1	59.6	1.2	1.5	3.5	13.4	--	0.2	70	
DRONE-PITCH	3.4	8.7	--	0.2	0.7	9.1	--	0.1	13	
DRONE-YAW	8.0	15.4	--	0.6	0.9	17.4	--	0.1	25	
GLIDE BOMB-PITCH	24.0	44.8	0.7	1.4	2.5	13.5	0.1	0.2	53	
GLIDE BOMB-YAW	55.3	57.4	14.2	8.6	3.7	19.4	0.1	0.7	84	

INPUT VALUES FOR ERROR ANALYSIS

	<u>DETERMINISTIC</u>	<u>STOCHASTIC</u>
SENSOR	1.00 DEG	0.08 (DEG) <sup>2</sup> /HZ
WIND	0.50 FT/SEC/100 FT	10.0 FT/SEC (RMS)
ACCEL	1.00 FT/SEC <sup>2</sup>	0.025 (FT/SEC <sup>2</sup> ) <sup>2</sup> /HZ
GYRO	0.35 DEG/SEC	1.5 x 10 <sup>-4</sup> (DEG/SEC) <sup>2</sup> /HZ

(1) MISS DISTANCE IN FT (1σ) TYPICAL

TABLE 3.4

ERROR SENSITIVITIES

LOOP GAIN REDUCED 25 %

PROPORTIONAL NAVIGATION

VEHICLE	DETERMINISTIC (2)				STOCHASTIC (3)				ZERO ERROR (4)
	SENSOR	WIND	ACCEL	GYRO	SENSOR	WIND	ACCEL	GYRO	
MISSILE	0.6	0.2	0.3	10.4	274	12.2 (5)	--	114	0.17
PROJECTILE	0.7	0.1	0.2	3.8	351	5.6	--	118	0.15
DRONE-PITCH	0.2	0.2	0.1	2.3	14	13.5	--	4.4	0.11
DRONE-YAW	--	0.5	--	6.1	20	9.4	--	13.5	0.02
GLIDE BOMB-PITCH	0.1	0.1	0.1	2.3	1250	87	0.3	437	0
GLIDE BOMB-YAW	34	1.8	8.7	109	2230	1138	6.2	6150	5.94

PURSUIT NAVIGATION

VEHICLE	DETERMINISTIC (2)				STOCHASTIC (3)				ZERO ERROR (4)
	SENSOR	WIND	ACCEL	GYRO	SENSOR	WIND	ACCEL	GYRO	
MISSILE	30.6	105	0.8	2.8	119	0.67	0.1	1.2	1.0
PROJECTILE	37.9	124	1.6	5.8	167	0.75	--	2.2	1.6
DRONE-PITCH	4.0	20	--	1.0	7	0.12	--	0.4	0
DRONE-YAW	9.6	34	0.8	2.0	11	0.41	--	0.7	0.7
GLIDE BOMB-PITCH	26.3	95	0.8	5.7	95	0.68	0.2	4.0	0.7
GLIDE BOMB-YAW	56.9	117	15.1	27.3	177	1.29	0.7	47.7	18.8

NOTES:

(1) INPUT VALUES FOR SENSITIVITY ANALYSIS

	DETERMINISTIC	STOCHASTIC
SENSOR	1 DEG	1 DEG <sup>2</sup> /HZ
WIND	1 FT/SEC/100 FT	1 FT/SEC (RMS)
ACCEL	1 FT/SEC <sup>2</sup>	1 (FT/SEC <sup>2</sup> ) <sup>2</sup> /HZ
GYRO	1 DEG/SEC	1 (DEG/SEC) <sup>2</sup> /HZ

- (2) MISS DISTANCE FT (1σ)
- (3) MISS DISTANCE FT<sup>2</sup>/SPECTRUM LEVEL
- (4) MISS DISTANCE FT
- (5) x 10<sup>-4</sup> FT<sup>2</sup>/SPECTRUM LEVEL
- (6) INITIAL CONDITION 10 FT/SEC FOR DETERMINATION CALCULATION

In order to obtain a measure of the sensitivity to the gain level, a second case was run in which the overall navigation gain was reduced by 25%. The results of this calculation are shown in Table 3.4. As for Table 3.2, the two sections give the basic sensitivities for pursuit and proportional, respectively. In Table 3.5, the two sections give the error budget to the specified input values as before. Comparing the zero error case for the two gain levels, it may be seen that the only substantial change was for the GBU-yaw case for proportional, in which the miss distance was somewhat increased.

Looking at the individual error sensitivities, we see that for the proportional case that error sensitivities for sensor and gyro noise were substantially decreased, while the sensitivity for gyro bias was noticeably increased. The acceleration noise sensitivity was also somewhat increased, but it was quite low in any event. For the pursuit law, there was a slight degradation for all contributors. The total effect was a slight decrease in the RSS error for the proportional case and a slight increase in the error for pursuit case. Thus, we may conclude that both laws can perform adequately for substantial changes in gain from the nominal.

TABLE 3.5

ERROR SUMMARY

LOOP GAIN REDUCED 25%

PROPORTIONAL NAVIGATION

STOCHASTIC

VEHICLE	<u>DETERMINISTIC</u>				<u>STOCHASTIC</u>				
	SENSOR	WIND	ACCEL	GYRO	SENSOR	WIND	ACCEL	GYRO	RSS
MISSILE	0.7 (1)	0.1	0.3	3.8	4.7	0.6	--	--	6.1
PROJECTILE	0.7	--	0.2	1.4	5.3	0.4	--	--	5.5
DRONE-PITCH	0.2	0.1	0.1	0.8	1.1	1.1	--	--	2.8
DRONE-YAW	--	0.3	--	2.2	1.3	0.9	--	--	2.7
GLIDE BOMB-PITCH	0.1	--	0.1	0.8	10.0	1.6	--	--	10.2
GLIDE BOMB-YAW	34	0.9	8.7	39.3	13.4	5.8	0.4	--	54.7

PURSUIT NAVIGATION

STOCHASTIC

VEHICLE	<u>DETERMINISTIC</u>				<u>STOCHASTIC</u>				
	SENSOR	WIND	ACCEL	GYRO	SENSOR	WIND	ACCEL	TYRO	RSS
MISSILE	30.6	52.9	0.8	1.0	3.1	13.1	--	--	62.6
PROJECTILE	37.9	62	1.6	2.1	3.7	13.0	--	--	74.0
DRONE-PITCH	4.0	10.1	--	0.4	0.7	10.6	--	--	15.2
DRONE-YAW	9.6	16.8	0.8	1.1	1.0	19.1	--	--	27.2
GLIDE BOMB-PITCH	26.3	47.3	0.8	2.1	2.8	14.3	0.1	--	56.1
GLIDE BOMB-YAW	56.9	58.4	15.1	9.8	3.8	19.4	0.1	--	85.8

INPUT VALUES FOR ERROR ANALYSIS

SENSOR	1.00 DEG	0.080 (DEG) <sup>2</sup> /HZ
WIND	0.50 FT/SEC/100 FT	10.0 FT/SEC(RMS)
ACCEL	1.00 FT/SEC <sup>2</sup>	0.025 (FT/SEC <sup>2</sup> ) <sup>2</sup> /HZ
GYRO	0.35 DEG/SEC	1.5 x 10 <sup>-4</sup> (DEG/SEC) <sup>2</sup> /HZ

(1) MISS DISTANCE IN FT (1σ) TYPICAL

#### 4.0 CONCLUSIONS

The following observations can be made from the numerical results of this study:

1. The peak accelerations are generally higher for the pursuit law. This means that the potential for saturation of the maneuver capability of vehicle is more likely. In addition, a greater velocity loss can be expected from the pursuit law.
2. The largest error contributors for pursuit navigation are sensor bias, wind shear, and wind gust. On the other hand, the proportional law is relatively insensitive to wind effects.
3. The largest error contributors for the proportional law are sensor noise and gyro bias. The contribution of gyro bias arises from the need to subtract body rate from the strap-down sensor measurement. The larger sensitivity of the proportional law to sensor noise is basically due to the fact that noise is differentiated. On the other hand, for this same reason, the pursuit law is relatively insensitive to sensor and gyro noise.
4. The Mini Drone vehicle with proportional guidance produced the best performance with respect to miss distance in this study. In this case, even sensor and gyro contributions were small. The basic reason for this is that the Mini Drone vehicle is highly maneuverable. On the other hand, its slow speed may make it undesirable for some applications.
5. A reduction in the gains of both proportional and pursuit laws resulted in some degradation of the response. For proportional law, the gain reduction reduced the sensitivity to gyro and sensor noise, but increased the sensitivity to gyro bias.

These observations support the following conclusions:

- For accurate results in closed loop simulations of systems with proportional navigation, the simulations should include the effects of gyro and sensor noise. For simulations involving pursuit law, accurate simulations should include the effects of the wind (both shear and gust) as well as any bias in the sensor.

- The numerical results and the above associated observations support the conclusion that a proportional based law is generally more effective than a pursuit based law.
- In the implementation of a strapdown sensor for proportional navigation a gyro of less noise and drift than the usual autopilot sensors may be needed.

Closed loop simulations [6] of these vehicles with a more accurate representation of the aerodynamic parameters as well as saturation limitations tend to support the conclusions with respect to the superiority of the proportional navigation law. It was found in this study that the use of a "noise adaptive" gain in conjunction with the proportional navigation law greatly improved the performance of the systems. The noise adaptive gain mechanization was expressed as

$$G_A = \frac{G}{1 + \frac{V}{V_0}}$$

$$\text{where } V = \sum_{i=N-n_0}^{i=N} (\dot{\lambda}_i - \bar{\dot{\lambda}})^2$$

$N$  = current time interval

$n_0$  = no of samples in window

$\dot{\lambda}_i$  =  $i$ th value of LOS rate

$\bar{\dot{\lambda}} = \frac{1}{n_0} \sum_{i=N-n_0}^{i=N} \dot{\lambda}_i$  average value of the LOS rate in window

$V_0$  = reference variance

$G_A$  = noise adjusted gain

$G$  = nominal gain

For periods of very high noise levels, this law was quite effective in reducing the loss in energy produced by noise induced maneuver drag. Since the present studies show that a reduction in gain reduces the sensor noise contribution to miss distance, this should also provide some insulation against degradation

caused by sensor noise. Care must be taken, however, that a proper balance is struck since a reduction in gain also produces an increase in contribution of gyro drift.

Since the noise adaptive gain is relatively easy to implement in a system, development of methods for optimizing its parameters  $V_0$  and  $n_0$  would be a good direction in which to proceed.

## REFERENCES

1. I.G. Stiglitz, "A Precision Guided Weapons System Concept for Command and Control Countermeasures," Project Report TST-40, Lincoln Laboratory, M.I.T., (26 July 1979).
2. D.V. Stallard, "Classical and Modern Guidance of Homing Interceptor Missiles," Raytheon Company, Missile Systems Division, Bedford, MA (April 1968), p. 247.
3. P. Garnell, D.J. East, Guided Weapon Control Systems (Pergamon Press, New York, 1977).
4. R.S. Warren, C.F. Price, A. Gelb, and W.E. Vandervelde, "Direct Statistical Analysis of Non-Linear Guidance Systems," AIAA Guidance and Control Conference, 1973.
5. P. Zarchan, "Complete Statistical Analysis of Non-Linear Guidance Systems - SLAM," AIAA Guidance and Control Conference, 1977.
6. R. D'Amato, J. Capon, C. Sorrentino, "Digital Simulation of Several Flight Vehicles," Project Report, Lincoln Laboratory, M.I.T. (In Preparation).
7. C.E. Mueller, R.K. Phelps, R. Scheidenhelm, "Tactical Guidance Requirements for Strapdown Inertial," NAECON 77 RECOFD.
8. Northrop Corporation, Precision Products Division, Private Communication.

UNCLASSIFIED

SECURITY CLASSIFICATION OF THIS PAGE (When Data Entered)

19 REPORT DOCUMENTATION PAGE		READ INSTRUCTIONS BEFORE COMPLETING FORM	
1. REPORT NUMBER (18) ESD TR-80-68	2. GOVT ACCESSION NO. AD-A090 155	3. RECIPIENT'S CATALOG NUMBER	
4. TITLE (and subtitle) (6) Error Analysis of Pursuit and Proportional Navigation Control Laws,		5. TYPE OF REPORT & PERIOD COVERED (9) Project Report,	
7. AUTHOR(s) (10) Richard D'Amato		6. PERFORMING ORG. REPORT NUMBER Project Report TST-43	
(14) TST-43		8. CONTRACT OR GRANT NUMBER(s) (15) F19628-80-C-0002	
9. PERFORMING ORGANIZATION NAME AND ADDRESS Lincoln Laboratory, M. I. T. P. O. Box 73 Lexington, MA 02173		10. PROGRAM ELEMENT, PROJECT, TASK AREA & WORK UNIT NUMBERS Program Element No. 63601F Project No. 670B	
11. CONTROLLING OFFICE NAME AND ADDRESS Air Force Systems Command, USAF Andrews AFB Washington, DC 20331 (12) 45		12. REPORT DATE (11) 28 Jan 1980	
14. MONITORING AGENCY NAME & ADDRESS (if different from Controlling Office) Electronic Systems Division Hanscom AFB Bedford, MA 01731		13. NUMBER OF PAGES 46	
		15. SECURITY CLASS. (of this report) Unclassified	
		15a. DECLASSIFICATION DOWNGRADING SCHEDULE	
16. DISTRIBUTION STATEMENT (of this Report)  Approved for public release; distribution unlimited.			
17. DISTRIBUTION STATEMENT (of the abstract entered in Block 20, if different from Report)			
18. SUPPLEMENTARY NOTES  None			
19. KEY WORDS (Continue on reverse side if necessary and identify by block number)  error analysis      emitter homing simulations      airframe      autopilot			
20. ABSTRACT (Continue on reverse side if necessary and identify by block number)  A comparative study of pursuit and proportional navigation laws to be used in emitter homing simulations is made for several types of flight vehicles. The framework for this study, although relatively simple, includes the essential features of the two control laws, such as the aero/inertial characteristics of the airframe and the important parameters of the autopilot. Both deterministic and stochastic error models of wind, sensor, gyro, and accelerometer are considered. The main conclusions of the study are that gyro bias and sensor noise are dominant for proportional, while wind and sensor bias are most important for pursuit. Proportional was found to be more effective than pursuit, but implementation of proportional with a strapdown sensor may require a more accurate gyro than usually required by an autopilot.			

DD FORM 1 JAN 73 1473 EDITION OF 1 NOV 65 IS OBSOLETE

UNCLASSIFIED  
SECURITY CLASSIFICATION OF THIS PAGE (When Data Entered)

207650

MA